

# Journal of Biological Rhythms

<http://jbr.sagepub.com/>

---

## Wavelet-Based Time Series Analysis of Circadian Rhythms

Tanya L. Leise and Mary E. Harrington

*J Biol Rhythms* 2011 26: 454

DOI: 10.1177/0748730411416330

The online version of this article can be found at:

<http://jbr.sagepub.com/content/26/5/454>

---

Published by:



<http://www.sagepublications.com>

On behalf of:



<http://www.srbbr.org>  
Society for Research on Biological Rhythms

**Additional services and information for *Journal of Biological Rhythms* can be found at:**

**Email Alerts:** <http://jbr.sagepub.com/cgi/alerts>

**Subscriptions:** <http://jbr.sagepub.com/subscriptions>

**Reprints:** <http://www.sagepub.com/journalsReprints.nav>

**Permissions:** <http://www.sagepub.com/journalsPermissions.nav>

**Citations:** <http://jbr.sagepub.com/content/26/5/454.refs.html>

>> [Version of Record](#) - Sep 15, 2011

[What is This?](#)

# Wavelet-Based Time Series Analysis of Circadian Rhythms

Tanya L. Leise<sup>\*1</sup> and Mary E. Harrington<sup>†</sup>

<sup>\*</sup>*Department of Mathematics, Amherst College, Amherst, MA,*  
and <sup>†</sup>*Neuroscience Program, Smith College, Northampton, MA*

**Abstract** Analysis of circadian oscillations that exhibit variability in period or amplitude can be accomplished through wavelet transforms. Wavelet-based methods can also be used quite effectively to remove trend and noise from time series and to assess the strength of rhythms in different frequency bands, for example, ultradian versus circadian components in an activity record. In this article, we describe how to apply discrete and continuous wavelet transforms to time series of circadian rhythms, illustrated with novel analyses of 2 case studies involving mouse wheel-running activity and oscillations in PER2::LUC bioluminescence from SCN explants.

**Key words** wheel running, SCN, period variability, amplitude variability, frequency bands, discrete wavelet transform, analytic wavelet transform

Circadian rhythms are characterized by approximately 24-hour cycles of some observable variables such as locomotor activity or clock gene expression. The period of some rhythms can be quite precise, for example, the cyanobacteria *Synechococcus elongatus* (Mihalcescu et al., 2004), but circadian oscillations can also exhibit considerable variability in period and amplitude over time. Here, we describe cases where period and/or amplitude vary over time and for which wavelet analysis provides a means to describe aspects of the data that cannot be obtained through more traditional methods. Wavelet transforms can be applied to directly measure period and amplitude as they vary over time in an activity record or bioluminescence time series. Alternatively, they can be used to eliminate noise and trend from time series to facilitate estimation of phase markers such as peak time. Wavelet methods can also be used to assess the strength of signal components lying in different frequency bands, for example, ultradian versus circadian components of an activity record. In this article, we provide a full description of this new

approach with information that will allow researchers with similar requirements to apply wavelet analysis to their data.

Wavelet analysis has been previously applied to the field of chronobiology in a few instances, for example, to study ultradian activity rhythms (Poon et al., 1997; Chan et al., 2000) and to decompose *Drosophila* mating songs (Dowse, 2009). Price et al. (2008) and Baggs et al. (2009) used continuous wavelet transforms with ridges to analyze cell luminescence data. Etchegaray et al. (2010) used a similar wavelet analysis to analyze regulation of circadian period length by casein kinase 1 $\delta$  in mouse SCN neurons. Meeker et al. (2011) applied wavelet analysis to analyze period instability in SCN neurons. Here, we provide further examples to demonstrate cases where this approach is helpful, and we provide background and methods directed toward the circadian researcher new to the application of wavelet analysis. Technical material is separated from the main text into 4 boxes: Box 1 describes nonstationary signals, Box 2 briefly reviews Fourier analysis of time

1. To whom all correspondence should be addressed: Tanya L. Leise, Department of Mathematics, Amherst College, Amherst, MA 01002; e-mail: tleise@amherst.edu.

series, Box 3 defines the discrete wavelet transform, and Box 4 explains the analytic wavelet transform. After a basic introduction describing wavelet analysis, we present 2 case studies to illustrate how these methods go beyond more traditional methods of analysis.

**INTRODUCTION TO WAVELET ANALYSIS**

Accurate determination of period length is critical for most circadian studies. Common techniques including the Fourier periodogram, sine wave fitting, maximum entropy spectral analysis (MESA), and

**Box 1. Nonstationary Signals**

Sinusoids are the canonical periodic signals. For example, the signal

$$x(t) = A \cos\left(\frac{2\pi}{\tau}(t - t_0)\right)$$

oscillates with frequency  $2\pi/\tau$ , equivalent to a period of  $\tau$ , has amplitude  $A$ , and peaks at time  $t_0$  (and every  $\tau$  time units thereafter). In contrast, the period and amplitude of nonstationary signals vary over time. An oscillatory signal that may vary in amplitude and frequency over time has generic form

$$x(t) = a(t)\cos\theta(t).$$

For instance, the frequency of the signal

$$x(t) = A \cos\left(\frac{2\pi}{\tau_c} t + \frac{\tau_m \Delta f}{2\pi} \sin\left(\frac{2\pi}{\tau_m} t\right)\right)$$

varies around a central frequency of  $2\pi/\tau_c$  by  $\pm\Delta f$  every  $\tau_m$  time units. The instantaneous frequency of such signals is the derivative  $\theta'(t)$  of the phase function. In the case of a fixed frequency signal with  $\theta(t) = 2\pi t/\tau$ , the derivative is  $2\pi/\tau$ , and so the instantaneous frequency agrees with the usual definition of frequency. We can also vary the amplitude  $a(t)$  over time, for example,

$$x(t) = \left( A + \Delta A \cos\left(\frac{2\pi}{\tau_m} t\right) \right) \cos\left(\frac{2\pi}{\tau}(t - t_0)\right).$$

See chapter 4 of Mallat (2009) for more details.

**Box 2. The Discrete Fourier Transform (DFT)**

A central objective of discrete Fourier and wavelet analysis is to express a signal as a sum of waveforms. Fourier analysis utilizes cosines and sines of different frequencies, conveniently expressed mathematically as  $e^{2\pi ikt} = \cos 2\pi kt + i \sin 2\pi kt$ , where  $i = \sqrt{-1}$ . Suppose a signal  $x = \{x_k\}$  is created by measuring some quantity every  $\Delta t$  hours for a total of  $N$  measurements labeled  $x_0, x_1, \dots, x_{N-1}$ , so that  $x_n$  corresponds to time  $t = n\Delta t/N$ . The DFT coefficient  $X_k$  of  $x$  is defined to be

$$X_k = \sum_{n=0}^{N-1} x_n e^{-2\pi ikn/N}.$$

The fast Fourier transform (FFT) is a very efficient algorithm used to compute the DFT of signals for which  $N$  is a power of 2, but the DFT may be applied to signals of any length  $N$ . The adjusted Fourier coefficient  $X_k/N$  is the amplitude associated with component  $e^{2\pi ikt}$ ; that is, the DFT allows us to decompose the original signal into a sum of sinusoidal components:

$$x_n = \frac{1}{N} \sum_{k=0}^{N-1} X_k e^{2\pi ikn/N}.$$

The sinusoidal functions of Fourier analysis are excellent for determining what frequencies are present in a signal, but because sinusoids oscillate at a fixed frequency for all time, they cannot be used to assess how the period of a signal varies over time. Figure 1 illustrates these ideas. For more details, see chapter 3 of Mallat (2009).

autocorrelation-based methods assume that the intrinsic period and amplitude do not change over time, as is true for stationary time series. These methods yield good results for most experimental data when applied appropriately, with the best choice of method depending

on the characteristics of the particular time series. The resolution of the Fourier periodogram, which is essentially the discrete Fourier transform (DFT), depends on the number of cycles contained in the data and so requires a relatively long record (typically at least 10

### Box 3. The Discrete Wavelet Transform (DWT)

Wavelet transforms typically involve waveforms that have finite support, that is, are nonzero on a finite length interval, in contrast to cosines and sines that oscillate for all time. Whereas the DFT decomposes a signal  $x$  into a sum of sinusoids at particular frequencies, the DWT splits  $x$  into components called wavelet details and smooths that are associated with different frequency bands. This is accomplished by repeatedly applying a high-pass wavelet filter (HPF) to generate wavelet coefficients  $W_{j,k}$  and a low-pass scaling filter (LPF) to generate scaling coefficients  $V_{j,k}$ . See Figure 2 for graphs of the wavelet and scaling filters used in this article.

The wavelet coefficients  $W_{j,k}$  yield the level  $j$  wavelet detail  $D_j$ , and the scaling coefficients  $V_{j,k}$  yield the level  $j$  wavelet smooth  $S_j$ , via application of the inverse DWT. The original signal  $x$  is the sum of the wavelet details  $D_1, \dots, D_J$  plus the final wavelet smooth  $S_J$ , where  $J$  is the number of levels computed. Figure 2 illustrates this process for  $J = 3$ . The wavelet detail  $D_j$  corresponds to a frequency band with period range  $2^j\Delta t$  to  $2^{j+1}\Delta t$  time units, where the signal  $x$  was created by sampling every  $\Delta t$  time units. Hence, each level is associated with a scale twice as long as the previous level's. The wavelet smooth  $S_j$  is obtained by repeated smoothing via the LPF and so forms the trend of the signal. Together, the wavelet details and smooth form a multiresolution analysis (MRA) of the signal, exemplified in Supplementary Figure S2 for bioluminescent signals. We use a translation-invariant DWT (also known as a stationary or maximal overlap DWT) that does not downsample like the regular form of the DWT. For more information, see Percival and Walden (2000).

### Box 4. The Analytic Wavelet Transform (AWT)

In contrast to the DWT that uses a pair of real-valued filters, the AWT involves a complex-valued wavelet function  $\psi(t)$  that corresponds to a frequency band determined by its DFT, as illustrated in Figure 3 for the Morse wavelet function. The AWT of a signal  $x(t)$  at time  $t$  and scale  $s$  is defined to be

$$W(t, s) = \int_{-\infty}^{\infty} \frac{1}{s} \psi^* \left( \frac{u-t}{s} \right) x(u) du,$$

where the asterisk denotes the complex conjugate (reverses the sign of the imaginary part). Essentially, the wavelet transform correlates the given signal  $x(t)$  with wavelet functions that have been translated to be centered at time  $t$  and scaled by a factor  $s$  (thereby altering the period). At a given time  $t$ , we identify the period of the signal by finding the scale that maximizes the wavelet transform (hence, the correlation) between the signal and the scaled wavelet. This is the idea behind the wavelet ridge, which estimates the instantaneous frequency and amplitude of the signal at each time point. Wavelet ridge curves run along local maxima with respect to  $s$  (for each fixed  $t$ ) of the absolute value of the AWT and thereby indicate the signal's instantaneous frequency and analytic amplitude at each time point, as shown in Supplementary Figure S5 for 2 examples. We use bandpass normalization, as described in Lilly and Olhede (2009), so that  $|W(t, s)|$  can be directly interpreted as amplitude. The transform essentially finds the correlation between the signal and the wavelet function, and the ridge curve identifies the waveforms that have the greatest correlation with the signal. The scale  $s$  can be interpreted as frequency via  $\omega = \varphi/s$  or as period via  $\tau = 2\pi s/\varphi$ , where  $\varphi$  is the mean frequency of the wavelet function  $\psi(t)$ . The AWT also yields phase information because each complex number  $z = re^{i\theta}$  encodes both amplitude  $r$  and phase angle  $\theta$ .

Another way to understand what the AWT does is to examine the transform's action in the frequency domain, in the same way we examine how filtering works in Supplementary Figure S1. We can reformulate the definition of  $W(t, s)$  to work in the frequency domain rather than in the time domain:

$$W(t, s) = \frac{1}{2\pi} \int_{-\infty}^{\infty} \frac{1}{s} \Psi^*(s\omega) X(\omega) e^{i\omega t} d\omega,$$

where  $X(\omega)$  and  $\Psi(\omega)$  are the Fourier transforms of  $x(t)$  and  $\psi(t)$ , respectively. This says that the AWT is in effect multiplying the signal's frequency spectrum by the wavelet function's Fourier transform  $\Psi$  (Fig. 3). Changing  $s$  shifts  $\Psi(s\omega)$  along the frequency axis, and the ridge location corresponds to the value of  $s$  that maximally matches  $\Psi(s\omega)$  with the signal's frequency profile  $X(\omega)$ . See Lilly and Olhede (2010), Selesnick et al. (2005), and chapter 4 of Mallat (2009) for further information about the AWT.

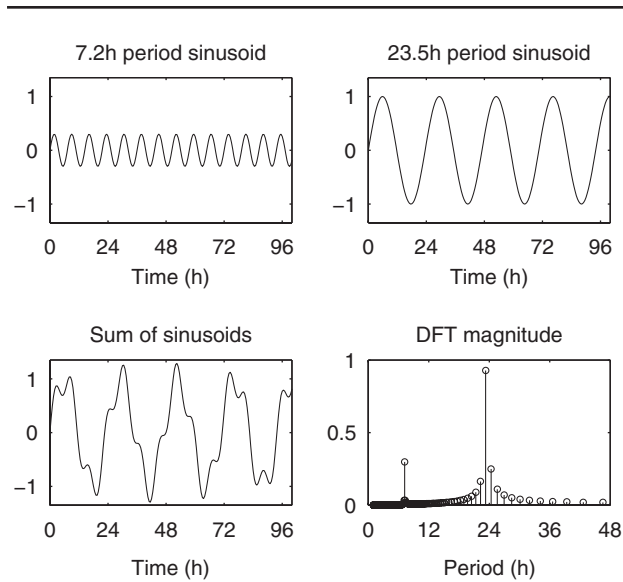


**Figure 1.** Example of the DFT applied to a simple oscillatory signal. We sum 2 sinusoids with periods of 7.2 hours and 23.5 hours to obtain a signal  $x$ . The DFT coefficients' magnitudes,  $|X_k|/N$ , give the amplitude of the sinusoids with frequencies  $k/N$ , whose sum will equal the signal  $x$  (in this example,  $N = 1024$ ) (see Box 2). The 2 peak DFT coefficients closely match the periods and amplitudes of the 2 sinusoids, but with "leakage" around the peak frequency due to the DFT frequency corresponding to 23.3 hours, slightly different from the signal's period of 23.5 hours. The resolution of the DFT depends on the number of cycles present in the signal; if the signal's peak frequency does not exactly match one of the DFT's frequencies, the DFT must use a combination of nearby frequencies to match the signal.

cycles). Autocorrelation yields a period estimate with resolution that depends on the sampling interval and is best applied to records with at least 4 cycles and a short sampling interval. MESA has finer resolution than the Fourier periodogram and works reasonably well even for short, noisy time series as long as the period and amplitude do not vary significantly over time. Unlike the previous 3 methods, sine wave fitting is not restricted to a grid of periods and can be applied to short time series (3 or more cycles for good results), but it is more sensitive to variations in period and amplitude. See Levine et al. (2002) and Dowse (2009) for further details on these commonly used methods for circadian data.

While performing well in many circumstances, traditional methods can be unreliable when applied to data with significant variation in amplitude and period across cycles, that is, nonstationary time series (Box 1), and none of them measures how the period may be changing over time within a time series. Because circadian data are often nonstationary (Refinetti, 2004), these traditional methods may be inadequate in some cases, and wavelet-based approaches may prove more effective for determining period length as well as

offering a means of measuring variability in period and amplitude within a time series.

Wavelet analysis, similar to Fourier analysis, attempts to express a signal as a sum of component waveforms. Whereas the waveforms in Fourier analysis are sines and cosines of a set of fixed frequencies (Box 2 and Fig. 1), wavelet transforms allow us to decompose a signal in a more flexible manner. In addition to being the method of choice for analyzing nonstationary time series, wavelet analysis has some advantages over traditional methods; for example, wavelet methods do not require removal of noise or trend to accurately measure period. In fact, the discrete wavelet transform (DWT) can itself be a very effective tool to remove trend and noise from a time series by focusing on a desired frequency band, thereby facilitating clear and accurate identification of phase markers such as peaks. The DWT decomposes a time series into components corresponding to different frequency bands in a time-localized manner (Box 3, Fig. 2, and Suppl. Fig. S2), thereby isolating the circadian component to effectively remove trend and noise (Suppl. Fig. S3) as well as partitioning the variance of a time series according to the frequency band (Suppl. Fig. S4). In contrast, a type of complex-valued continuous wavelet transform called the analytic wavelet transform (AWT) directly measures period and amplitude varying over time in a time series (Box 4).

Wavelet functions are not periodic, so each wavelet function involves a band of frequencies rather than a single frequency, as illustrated in Figure 3. In switching from Fourier analysis, with its precise frequency determination but lack of time localization, to wavelet analysis, we gain time localization at a cost of some loss of precision in frequency. Because of this "smearing" of frequency content in wavelet functions, we refer to the scale of a wavelet. Each scale corresponds to a frequency band rather than to a single frequency. Large scales correspond to low frequencies (equivalently, long periods) and can be associated with the general trend of a signal, while very small scales correspond to high frequencies and are often associated with high-frequency noise.

The underlying idea behind using wavelet transforms like the AWT to measure period is as follows: Take a wavelet filter (for a discrete transform) or a wavelet function (for a continuous transform), and translate it along the time axis to center it at the time point of interest. Rescaling the wavelet allows us to assess a wide range of frequencies. Compute the correlation between each rescaled wavelet and the time series, and choose the scale that yields the largest correlation. We associate this scale with the mean frequency of the scaled wavelet's frequency band, thereby allowing us to assign a period

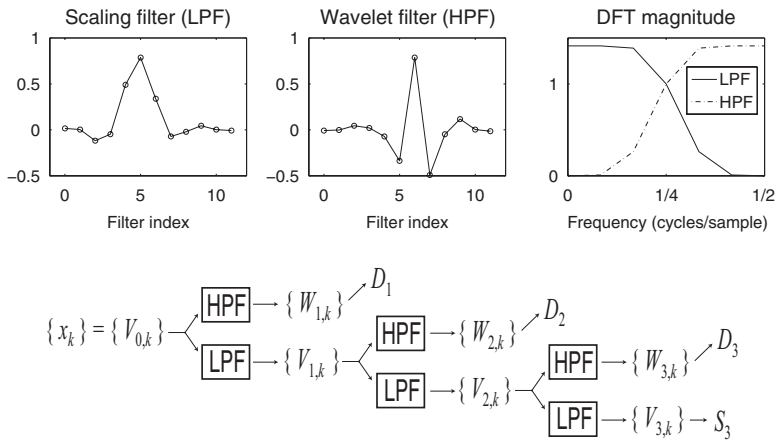


**Figure 2.** Filters associated with the DWT and the pyramid algorithm used to compute the DWT. Shown here are the Daubechies least-asymmetric wavelet and scaling filters of length 12, along with their DFTs. The wavelet filter is a high-pass filter (HPF) with a DFT magnitude greatest for high frequencies, and the scaling filter is a low-pass filter (LPF) with a DFT magnitude greatest for low frequencies. In the DFT graph, frequency is given in terms of cycles per sample, where the highest possible discernible frequency is one cycle per 2 samples (i.e., signal alternates values at every other time point). The scaling filter acts by multiplying the signal's DFT by the LPF DFT, thereby retaining only the low-frequency content of the signal. This complements the action of the wavelet filter, which multiplies the signal's DFT by the HPF DFT, thereby retaining only the high-frequency content. The pair of filters are applied repeatedly as shown in the diagram to yield wavelet coefficients  $W_{j,k}$  (used to generate wavelet detail  $D_j$ ) and scaling coefficients  $V_{j,k}$  (used to generate wavelet smooth  $S_j$ ). See Box 3 for further details.

to the time series at that time point. The AWT is particularly good for visualizing fluctuations in period as well as in amplitude. The AWT coefficients indicate the correlation between the scaled wavelets and the time series at each time point, often graphed as a heat map with a ridge marking maxima (highest correlation), thereby indicating the period of the time series at each point, as illustrated for simple examples in Supplementary Figure S5. Note that as a consequence of the fact that wavelets are associated with a frequency band rather than a single frequency, the AWT will not distinguish frequencies that are too close relative to the wavelet function's frequency spread. MESA (Dowse, 2009) can be applied to test whether a signal involves clustered frequencies, as this method can be effective at resolving closely spaced frequencies.

Wavelet methods have application beyond direct period measurement. A multiresolution analysis (MRA) uses the DWT to decompose a signal into components called details associated with different frequency bands and a smooth that can be treated as the trend (Box 3, Fig. 2, and Suppl. Fig. S2). The underlying idea here is to repeatedly apply a wavelet filter to extract details at different scales, while a scaling filter smooths the signal (analogous to a running average). This method can be used to remove noise and trend to yield a clean signal

for examining phase markers such as peaks, for example, in bioluminescence time series. In this manner, the DWT can enhance commonly used methods such as peak picking or sine wave fitting by optimally removing noise and trend from time series, as shown in Supplementary Figure S3. The MRA also partitions the energy of the signal with respect to scale, which can be used to characterize a rhythm or as a rhythmicity criterion by assessing what proportion of the rhythm's energy lies in a circadian range. Energy in this context equals the variance of the detrended time series; see Supplementary Section S.2 for a rigorous definition and Supplementary Figure S4 for cell data examples. Strong, coherent circadian rhythms are characterized by their energy being concentrated in the frequency band containing the period of the rhythm. This is analogous to how Ko et al. (2010) used the DFT to generate a rhythmicity criterion for SCN neurons by examining the proportion of power in the peak circadian frequency.

Wavelet transforms are powerful tools for assessing rhythmic data, but like the Fourier transform, they must be applied properly to yield valid results. Both Fourier and wavelet methods require time series to be of a minimum length to estimate period with good precision. A particular issue with wavelet transforms and other filtering methods is that of edge effects (distortions in the transformed or filtered signal near its beginning and end). When a wavelet transform is applied at a time  $t$  that is near the beginning or end of a time series, the wavelet function or filter runs off the edge, and we must choose a way of extending the time series to fully overlap. Common choices are to pad each end with zeros or with the mean value of the time series. Other choices that can reduce edge effects are to apply periodic boundary conditions (joining the ends to wrap around) or reflection boundary conditions (reflecting about each end) after adjusting the time series to start and end at peaks or troughs. A consequence of artificially extending the time series in any of these ways is that the wavelet transform will be distorted near the edges. It is best to ignore regions exhibiting edge effects, typically at least 1.5 days on each end for frequencies in the circadian range, unless careful measures are taken to minimize boundary distortions. This implies that the data series must cover substantially more than 3 days for wavelet methods to be useful in measuring circadian periods.

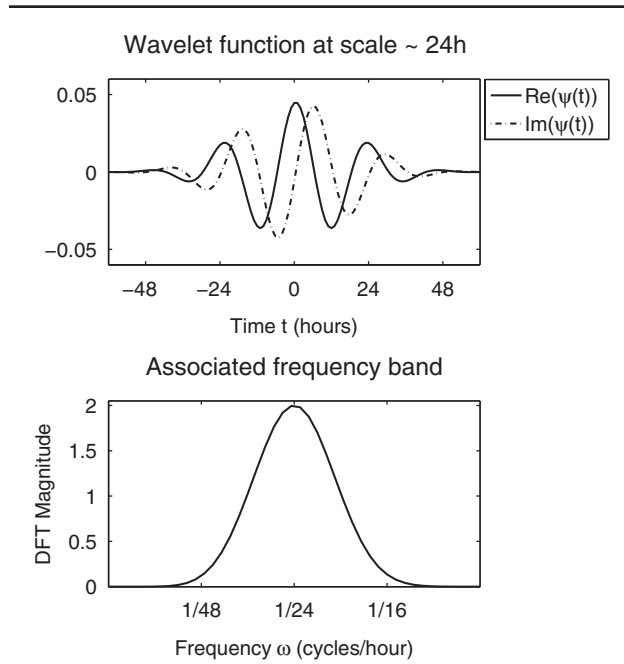


**Figure 3.** Morse wavelet function (with  $\beta = 7$  and  $\gamma = 3$ ) and its frequency band, used in the analytic wavelet transform in this article. The Morse wavelet function is complex valued, that is, has both real and imaginary parts, allowing it to extract both amplitude and phase information from the signal, which real-valued transforms cannot do. For more details, see Box 4.

We present 2 case studies to illustrate the application of wavelet transforms to circadian data. Case study #1 uses the DWT to characterize the differences between wheel-running rhythms in LD and LL and subsequent effects on SCN PER2::LUC rhythms, while case study #2 applies the AWT to measure period and amplitude modulation in wheel-running activity of a female mouse due to the estrous cycle.

#### CASE STUDY #1: WHEEL RUNNING AND PER2::LUC EXPRESSION IN LD AND LL

##### Background

Constant light disrupts circadian activity rhythms in mice, fragmenting activity bouts, reducing activity levels, and lengthening period (Daan and Pittendrigh, 1976). Ohta et al. (2005) reported that individual SCN neurons in animals housed under constant light continue oscillating but are desynchronized. We expected that constant light would provide a condition under which period and amplitude of the circadian rhythm would vary, so that this would be a case where wavelet analysis would allow greater insight than more traditional methods that assume a stationary signal. We applied wavelet methods to compare activity and bioluminescence records from mPer2<sup>Luc</sup> mice under LD 12:12 and LL conditions (see Fig. 4 for representative samples).

## Results

As shown in Figure 5A, activity of mice entrained to LD tends to be greater than activity in LL; the mean activity of male mice under LL is significantly different from that of male mice in LD and of female mice in LD or LL (multiple comparison test,  $F = 7.5$ ,  $p < 0.001$ ). To further characterize patterns in wheel running during LD and LL of male and female mice, we used the DWT to partition the energy between ultradian and circadian scales, as described in Supplementary Section S.2 and Supplementary Figure S4. Figure 5B shows the proportion of energy associated with each wavelet detail of mouse wheel-running MRAs (see Fig. 4B for representative samples). Activity in LD has most of its energy in the wavelet detail corresponding to a circadian range of periods (in this example,  $D_6$ ), while mice in LL display more fragmented activity, with energy distributed among the ultradian scales. Activity under LD 12:12 is characterized by strong consolidation, with energy in the wavelet detail  $D_6$  (corresponding to a circadian range of periods) significantly greater under LD than LL (multiple comparison test,  $F = 53$ ,  $p < 0.001$ ). In LL, female mouse activity is distributed among  $D_3$  to  $D_6$ , while male mouse activity tends to be fragmented and so predominantly in  $D_1$  to  $D_3$ . The period of activity of mice during LL was  $25.0 \pm 0.3$  hours (mean  $\pm$  standard deviation, MESA; mean period of males and females not significantly different).

We measured variability in period of PER2::LUC luminescence rhythms of SCN explants by applying a DWT to remove noise and trend (Suppl. Fig. S3), allowing clear discernment of peak times. We then used the standard deviation of 5 consecutive peak-to-peak times as the measure of period variability for each PER2::LUC record. We observed more variability in period following LL than following LD (2-sample  $t$  test for unequal variances,  $t = 5.6$ ,  $df = 18$ ,  $p < 0.001$ ) (Fig. 5C). As shown in Figure 5D, there is a significant negative correlation between period variability in the SCN explant PER2::LUC rhythms and the proportion of energy of wheel-running activity in the circadian scale ( $r = -0.67$ ,  $p < 0.001$ ). That is, greater period variability in the SCN is associated with more fragmenting of wheel-running activity.

## Discussion

The DWT is used here for 2 different purposes: 1) characterizing activity by calculating the energy in each wavelet detail of the wheel-running time series, and 2) removing trend and noise from bioluminescence time series to allow identification of peak times for measuring period variability. Male mice under LL are significantly less active than females and also display greater fragmenting of activity, quantified using

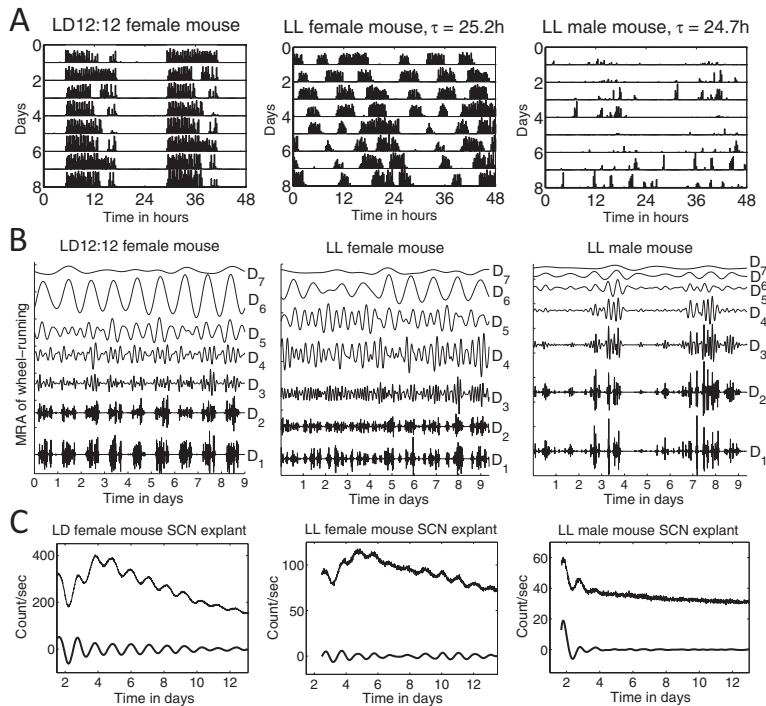


**Figure 4.** Representative examples of mice under LD 12:12 and LL conditions. (A) Double-plotted wheel-running records with 15-minute bins; periods were computed by MESA after subtracting the mean value. (B) Corresponding MRAs of the wheel-running records in A (smooth S, not shown); within each MRA, each detail has mean zero and is plotted with the same axis scaling, so magnitudes can be directly compared. (C) PER2::LUC bioluminescence of SCN explants from the mice whose activity records are shown in A, where graphs display both the raw signal and the signal with noise and trend removed via DWT.

wavelet analysis. All mice from LL showed more fragmented rhythms than mice from LD, resulting in most of the energy in activity under LL occurring in the ultradian scales (i.e., higher frequency bands). SCN explants from LL mice also exhibited greater variability in period. The correlation between variability of period in the SCN and fragmenting of locomotor activity suggests that the fragmentation of activity under LL may be partly attributable to destabilized rhythms in the SCN, consistent with the findings of Ohta et al. (2005). While some of these results may be clear by simply looking at the records, the wavelet analysis facilitates an objective quantitative evaluation of, for example, fragmenting of rhythms and variability in period, which is amenable to statistical analysis and can be applied to a wide variety of circadian data.

## CASE STUDY #2: EFFECTS OF ESTROUS CYCLE ON WHEEL-RUNNING RECORDS

### Background

The estrous cycle can affect the phase, period, and amplitude of rodent locomotor rhythms. Wollnik and

Turek (1988) found that the highest amplitude and activity bout length and the shortest circadian period length occurred on the day of estrus in rats for both LD 12:12-entrained and free-running animals. Estradiol shortens the period and advances the phase of wheel running in LD 12:12-entrained ovariectomized golden hamsters (Morin et al., 1977), while progesterone blocks the effects of estradiol on locomotor rhythms (Takahashi and Menaker, 1980). Janik and Janik (2003) found that the resetting of circadian rhythms through novel wheels can induce changes in the estrous cycle of Syrian hamsters. Pilorz et al. (2009) found that wheel-running activity was highest during estrus for wild-type and *Per1* mutant female mice but did not vary with the stage of the estrous cycle for *Per2* mutants, and Kopp et al. (2006) observed that the second part of the proestrous night was often characterized by increased activity in young female mice. These observed effects of the estrous cycle on locomotor patterns imply that female rodent wheel-running records should be treated as nonstationary time series, and wavelet analysis offers a means of objectively quantifying the variation in period, phase, and amplitude that occurs during the 4- to 5-day estrous cycle.

### Results

We examined the wheel-running record of a female *mPer2<sup>Luc</sup>* mouse that was 3 months old at the start of the 20-day record shown in Figure 6A. The animal was well entrained to the LD 12:12 cycle, as indicated by the Fourier periodogram (Fig. 6B) and MESA, both showing strong peaks at 24.0 hours. However, neither the Fourier periodogram nor MESA can reveal time-varying patterns in the period of the mouse's activity. Therefore, to assess possible fluctuations in period and amplitude over time, we applied an AWT to the wheel-running record shown in Figure 6A to yield the heat map shown in Figure 6C. The wavelet ridge is the best estimate of the instantaneous frequency and amplitude of the signal at each point (Box 4). In Figure 6D, we observe that the wavelet ridge displays a systematic 4- to 5-day variation in period and amplitude, and Supplementary Figure S6 shows the variation in phase angle over time.



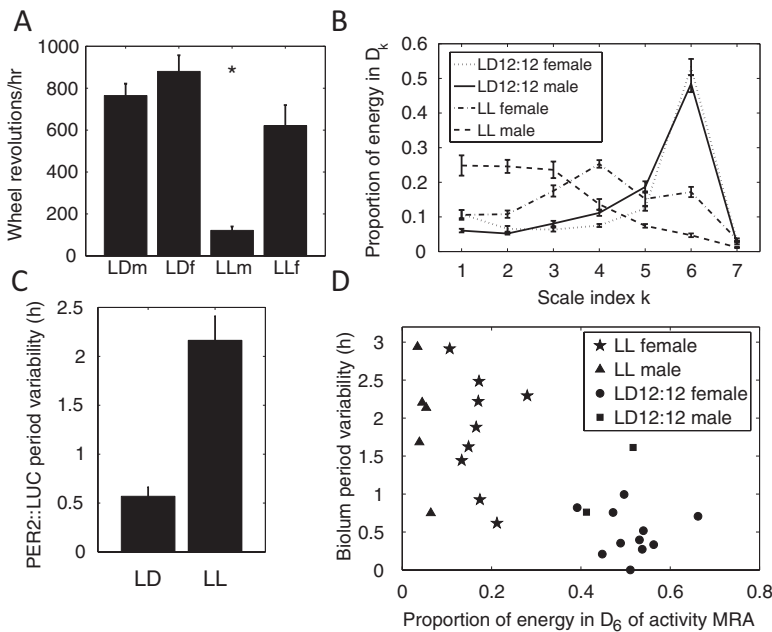


**Figure 5.** (A) Mean wheel-running activity under LD and LL conditions for male and female mice. Bars show mean  $\pm$  standard error. (B) Scale-based characterization of wheel-running activity under LD 12:12 and LL for male and female mice (23 LD 12:12 females, 8 LD 12:12 males, 9 LL females, 5 LL males). Error bars indicate mean  $\pm$  standard error. (C) Period variability of PER2::LUC bioluminescence rhythms in SCN explants, calculated as the standard deviation of 5 consecutive peak-to-peak times following LL and LD conditions. Bars indicate mean  $\pm$  standard error. (D) Graph showing PER2::LUC period variability versus the proportion of energy lying in the circadian component (wavelet detail  $D_6$ ) of wheel-running activity. A low proportion of energy in the circadian component of wheel running indicates fragmented activity patterns.

While the scalloping of activity can be discerned by the eye in some cases, the AWT provides a means of objectively quantifying the variation over time of period, amplitude, and phase that is associated with the 4- to 5-day estrous cycle. For example, Figure 6C suggests that the amplitude tends to be greatest while the period is growing shorter. We can use the wavelet ridge to more precisely quantify the relationship between period and amplitude variation. Autocorrelation yields a period of 4.1 days for the period and amplitude curves in Figure 6D, with the period rhythm leading the amplitude rhythm by 0.7 days. That is, the shortest period occurs about 0.7 days before the minimum amplitude. Similar patterns can be observed in the examples shown in Supplementary Figure S7.

**Discussion**

The AWT facilitates visualization as well as quantification of variation in period and amplitude over time. The wavelet ridge curve indicates the period,

phase, and amplitude at each time point, thereby providing a means of quantifying changes in these circadian properties over time. In this example, the AWT reveals a 4- to 5-day variation occurring in the amplitude, period, and phase of wheel running that is consistent with the literature concerning the effects of the estrous cycle on activity patterns. The main point of this case study is that the wavelet methods provide an objective way to quantify features of activity records such as recurring changes of period and amplitude. The AWT can also be applied to other types of circadian time series such as bioluminescence rhythms (Price et al., 2008; Baggs et al., 2009; Meeker et al., 2011), and a variety of wavelet functions are available that can be used to detect other types of features, for example, edge detection wavelets that can be applied to detect discontinuities such as activity onsets.

Although both are wavelet transforms, the DWT and AWT are quite different in nature and serve distinct purposes in our analyses. The DWT is real valued and systematically decomposes a signal into details and a smooth, which prove useful for removing noise and trend from a time

series (by isolating the circadian component) and for characterizing rhythmicity through partitioning the energy with respect to scale. The effectiveness of the DWT in removing trend and noise can then facilitate other methods such as peak picking to yield period information, but the DWT does not itself directly measure period or amplitude. In contrast, the AWT is complex valued and can directly yield high-resolution measurements of period, phase, and amplitude over time. The difference in these transforms is due to 2 main factors: discrete versus continuous and real valued versus complex valued. The DWT is a discrete transform designed to output components corresponding to fixed frequency bands that exactly add up to the original signal, while the AWT is a continuous transform that scans a range of possible period values in order to determine the best estimate. Real-valued transforms cannot encode both phase and amplitude, as complex-valued transforms can due to the combination of real and imaginary parts (Box 4). Each approach has its advantages and drawbacks. The AWT, for example, tends to

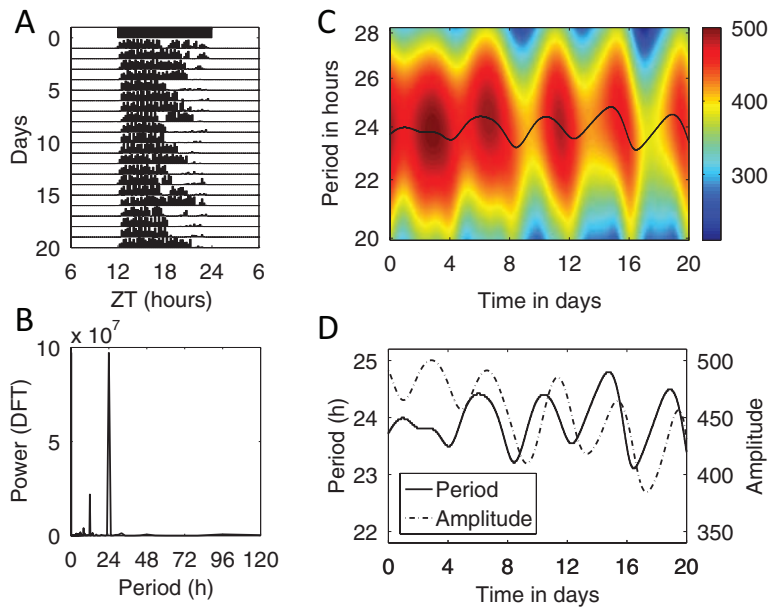


**Figure 6.** (A) Wheel-running activity of a young female mouse, double plotted with 15-minute bins, ranging from 0 to 1200 revolutions per bin. (B) Fourier periodogram of this wheel-running record. (C) Analytic wavelet transform of the wheel-running record. Color scale indicates amplitude of the activity rhythm (absolute value of AWT coefficients along the ridge, in wheel revolutions per 15-minute bin); double this value to obtain the peak activity level in units of wheel revolutions per 15-minute bin. (D) Replotted wavelet ridge curve showing period over time together with the corresponding amplitude, showing the relationship between the 5-day variation in period and amplitude of wheel running for this mouse. See Supplementary Figure S6 for a plot of the phase angle over time.

underestimate period variations because it essentially averages over several cycles, whereas the DWT/peak-picking method can yield accurate period variability estimates (as used in case study #1). See Selesnick et al. (2005) for an excellent discussion contrasting the DWT with complex-valued wavelet transforms.

## MATERIALS AND METHODS

### Experimental Data

Mice ( $mPer2^{Luc}$ , both homozygous and heterozygous) were housed from birth under constant light or under LD 12:12 in standard group housing. At 6 weeks of age, mice were moved to individual cages with running wheels, and activity was monitored for 2 to 3 weeks. Mice were then euthanized with halothane anesthesia, and SCN tissue was cultured as described in Guenther et al. (2009), with bioluminescence monitored using Lumicycle (Actimetrics, Wilmette, IL). The female mouse ( $mPer2^{Luc}$  heterozygous) analyzed in case study #2 was housed with a running wheel under a LD 12:12 cycle.

### Data Analysis

For case study #1, we applied a translation-invariant DWT to wheel-running records with 15-minute bins, using periodic boundary conditions and starting and ending in the middle of rest intervals to minimize edge effects. We chose the Daubechies least-asymmetric filter of length 12 after verifying that longer length filters did not alter the scale energy estimates. We observed that shorter filters reduce edge effects but can yield distorted energy estimates. We also applied this DWT to  $PER2::LUC$  bioluminescence time series (10-minute time steps) to extract the circadian component (sum of  $D_6$  and  $D_7$ , covering a period range of 11-43 hours) and then used this to determine times of peak luminescence in SCN explants for use in calculating period variability. For case study #2, we applied the AWT using a Morse wavelet function with  $\beta = 7$  and  $\gamma = 3$ . We chose the Morse wavelet rather than the Morlet wavelet used by Price et al. (2008), Baggs et al. (2009), Etchegaray et al. (2010), and Meeker et al. (2011) because it has some technical advantages over the Morlet wavelet (Lilly and Olhede, 2010). We discarded 1.5 days from each end of the AWT coefficients to avoid edge effects. For assessment of overall period in activity rhythms, we applied MESA to the raw 15-minute binned wheel-running data after subtracting the mean.

### Wavelet Software

Publicly available sources of wavelet analysis software to calculate the AWT (including ridges) are the *waveclock* package for the statistical program *R* (Price et al., 2008), which uses the Morlet wavelet and is aimed specifically at clock data, and the *jlab* package for MATLAB (Lilly, 2010), which includes a wider set of options and choice of Morlet or Morse wavelets. Free toolboxes of MATLAB scripts for the DWT and translation-invariant DWT include the *wmtsa* package written by Charles R. Cornish as a companion for Percival and Walden (2000) and the *WaveLab* package developed by a group at Stanford University (Buckheit et al., 2005). Data analysis in this article was done with custom scripts run in MATLAB 7.11.0 (The MathWorks, Natick, MA) that call routines from the *wmtsa* package and from *jlab*. For sample

MATLAB scripts applying wavelet analysis to circadian datasets and links to MATLAB-based wavelet toolboxes, go to <http://www.cs.amherst.edu/~tleise/CircadianWaveletAnalysis.html>.

### ACKNOWLEDGMENTS

The authors gratefully acknowledge John Davis (Dean of Academic Affairs, Smith College) and Gregory Call (Dean of Faculty, Amherst College) for funding undergraduates to work on this research, including Yordanka Kovacheva and Rose Weisshaar, who assisted in testing AWT methods in MATLAB, and Kayla Correia, who assisted with selecting data files. The authors thank Penny Molyneux for her assistance with the animal experiments and funding from the National Science Foundation (1051716) and the National Institutes of Health (00232373).

### CONFLICT OF INTEREST STATEMENT

The author(s) have no potential conflicts of interest with respect to the research, authorship: and/or publication of this article.

### NOTE

Supplementary material for this article is available on the *Journal of Biological Rhythms* website at <http://jbr.sagepub.com/supplemental>.

### REFERENCES

- Baggs JE, Price TS, DiTacchio L, Panda S, Fitzgerald GA, and Hogenesch JB (2009) Network features of the mammalian circadian clock. *PLoS Biol* 7:e52.
- Buckheit J, Chen S, Donoho D, Johnstone I, and Scargle J (2005) WaveLab 850. Available from: <http://www-stat.stanford.edu/~wavelab>.
- Chan FHY, Wu BM, Lam FK, Poon PWF, and Poon AMS (2000) Multiscale characterization of chronobiological signals based on the discrete wavelet transform. *IEEE Trans Biomed Eng* 47:88-95.
- Daan S and Pittendrigh CS (1976) A functional analysis of circadian pacemakers in nocturnal rodents. *J Comp Physiol* 106:267-290.
- Dowse HB (2009) Analyses for physiological and behavioral rhythmicity. In *Methods in Enzymology Vol. 454*, Johnson ML and Brand L, eds, pp 141-174. Burlington, MA: Academic Press.
- Etchegaray J-P, Yu EA, Indic P, Dallman R, and Weaver DR (2010) Casein kinase 1 delta (CK1 $\delta$ ) regulates period length of the mouse suprachiasmatic circadian clock in vitro. *PLoS One* 5(4):e10303.
- Guenther CJ, Bickar D, and Harrington ME (2009) Heme reversibly damps PERIOD2 rhythms in mouse suprachiasmatic nucleus explants. *Neuroscience* 164:832-841.
- Janik LY and Janik D (2003) Nonphotic phase shifting in female Syrian hamsters: interactions with the estrous cycle. *J Biol Rhythms* 18:307-317.
- Ko CH, Yamada YR, Welsh DW, Buhr ED, Liu AC, Zhang EE, Ralph MR, Kay SA, Forger DB, and Takahashi JS (2010) Emergence of noise-induced oscillations in the central circadian pacemaker. *PLoS Biol* 8(10):e1000513.
- Kopp C, Ressel V, Wigger E, and Tobler I (2006) Influence of estrus cycle and ageing on activity patterns in two inbred mouse strains. *Behav Brain Res* 167:165-174.
- Levine JD, Funes P, Dowse HB, and Hall JC (2002) Signal analysis of behavioral and molecular cycles. *BMC Neuroscience* 3(1):1.
- Lilly JM (2010) JLAB: MATLAB freeware for data analysis, version 0.91. Available from: <http://www.jmlilly.net/software.html>.
- Lilly JM and Olhede SC (2009) Higher order properties of analytic wavelets. *IEEE Trans Signal Process* 57:146-160.
- Lilly JM and Olhede SC (2010) On the analytic wavelet transform. *IEEE Trans Inf Theory* 56:4135-4156.
- Mallat S (2009) *A Wavelet Tour of Signal Processing: The Sparse Way*. Burlington, MA: Academic Press.
- Meeker K, Harang R, Webb AB, Welsh DK, Doyle FJ, Bonnet G, Herzog ED, and Petzold LR (2011) Wavelet measurement suggests cause of period instability in mammalian circadian neurons. *J Biol Rhythms* 26:353-362.
- Mihalcescu I, Hsing W, and Leibler S (2004) Resilient circadian oscillator revealed in individual cyanobacteria. *Nature* 430:81-85.
- Morin LP, Fitzgerald KM, and Zucker I (1977) Estradiol shortens the period of hamster circadian rhythms. *Science* 196:305-307.
- Ohta H, Yamazaki S, and McMahon DG (2005) Constant light desynchronizes mammalian clock neurons. *Nat Neurosci* 8:267-269.
- Percival DB and Walden AT (2000) *Wavelet Methods for Time Series Analysis*. New York: Cambridge University Press.
- Pilorz V, Steinlechner S, and Oster H (2009) Age and oestrus cycle-related changes in glucocorticoid excretion and wheel-running activity in female mice carrying mutations in the circadian clock genes *Per1* and *Per2*. *Physiol Behav* 96:57-63.
- Poon AMS, Wu BM, Poon PWF, Cheung E, Chan F, and Lam FK (1997) Effect of cage size on ultradian locomotor rhythms of laboratory mice. *Physiol Behav* 62:1253-1258.
- Price TS, Baggs JE, Curtis AM, Fitzgerald GA, and Hogenesch JB (2008) WAVECLOCK: wavelet analysis of circadian oscillations. *Bioinformatics* 24:2794-2795.
- Refinetti R (2004) Non-stationary time series and the robustness of circadian rhythms. *J Theor Biol* 227:571-581.
- Selesnick IW, Baranuik RG, and Kingsbury NG (2005) The dual-tree complex wavelet transform. *IEEE Signal Process Mag* 22:123-151.
- Takahashi JS and Menaker M (1980) Interaction of estradiol and progesterone: effects on circadian locomotor rhythm of female golden hamsters. *Am J Physiol Regul Integr Comp Physiol* 239:R497-R504.
- Wollnik F and Turek FW (1988) Estrous correlated modulations of circadian and ultradian wheel-running activity rhythms in LEW/Ztm rats. *Physiol Behav* 43:389-396.

Supplementary Online Material

*Wavelet-based time series analysis  
of circadian rhythms*

Tanya L. Leise\* and Mary E. Harrington†

\*Department of Mathematics, Amherst College, MA 01002, USA

†Neuroscience Program, Smith College, Northampton, MA 01063, USA

## S.1 The discrete Fourier transform and filtering

The discrete wavelet transform (DWT) is built upon filtering, so it is important to first understand the basic idea behind circular filters. The main goal is to alter the frequency content of a signal, typically by reducing undesired high or low frequencies. The discrete Fourier transform (DFT) reveals the frequency content of a signal, which can then be altered by multiplication with the DFT of a filter. In the example shown in Figure S1, the filter's DFT is shown as a red curve centered on the peak circadian frequency. The effect of this filter is to isolate the circadian component of the signal by diminishing frequencies to either side of the desired frequency. See the caption to Figure S1 for full details. In general, a filter is created by first determining its intended effect in the frequency domain (analogous to drawing the red curve in Figure S1), and then applying an inverse DFT to obtain the filter itself.

## S.2 Applications of the discrete wavelet transform

As explained in the main text, the DWT involves two filters, a high-pass wavelet filter that retains only high frequencies, and a low-pass scaling filter that retains only low frequencies (see Figure 2). The pair of filters are applied repeatedly in an efficient procedure for numerically calculating the DWT called the pyramid algorithm, leading to a sequence of details and a final smooth that form the multiresolution analysis (MRA), illustrated in Figure S2. Notice that the wavelet detail  $D_7$  is the circadian component in Figure S2; in general, which detail corresponds to a circadian range of periods is controlled by the sampling interval.

Because the DWT decomposes the signal into details and a smooth that correspond to difference frequency bands, it offers an effective means of removing trend and noise. The idea is to retain only the components of interest, which could be the circadian component by itself (e.g.,  $D_7$ ) or a sum of details to retain characteristics of the signal's waveform while removing trend and noise (e.g.,  $D_5 - D_7$ ). See Figure S3 for a comparison to commonly used methods of removing trend.

A further use of the DWT is to partition the variance with respect to scale. Here we prefer the nearly-equivalent term *energy* as better describing the quantity involved. The signal's variance  $\sigma_x^2$  equals the mean of squared values of the signal minus the square of the mean. According to Parseval's theorem, the sum of squared values equals the mean of the squared Fourier coefficients, which can be used to partition the variance with respect to frequency. The wavelet and scaling filters satisfy the same orthogonality conditions and so we have a similar result for the DWT (Percival and Walden, 2000). For clarity, we use the following norm notation:

for a signal  $\mathbf{x} = \{x_k\}$ ,  $k = 0, \dots, N - 1$ , let  $\|\mathbf{x}\|^2 = \sum_{k=0}^{N-1} x_k^2$ , with a similar interpretation of  $\|\mathbf{W}_j\|^2$  as the sum of squared level- $j$  wavelet coefficients  $W_{j,k}$  over  $k = 0, \dots, N - 1$ . With this notation, we can write  $\|\mathbf{x}\|^2 = \|\mathbf{V}_J\|^2 + \sum_{j=1}^J \|\mathbf{W}_j\|^2$ , and then use this to partition the variance of the signal, where  $\bar{\mathbf{x}}$  is the signal's mean:

$$\begin{aligned} \sigma_x^2 &= \frac{1}{N} \sum_{k=0}^{N-1} x_k^2 - \bar{x}^2 = \frac{1}{N} \|\mathbf{x}\|^2 - \bar{\mathbf{x}}^2 \\ &= \frac{1}{N} \|\mathbf{V}_J\|^2 + \frac{1}{N} \sum_{j=1}^J \|\mathbf{W}_j\|^2 - \bar{\mathbf{x}}^2 \\ &= \left( \frac{1}{N} \|\mathbf{V}_J\|^2 - \bar{x}^2 \right) + \frac{1}{N} \sum_{j=1}^J \|\mathbf{W}_j\|^2 \end{aligned}$$

The term  $\left( \frac{1}{N} \|\mathbf{V}_J\|^2 - \bar{x}^2 \right)$  corresponds to variance accounted for by the trend, while the sum over  $\|\mathbf{W}_j\|^2$  partitions the remaining variance among the wavelet details. We discard the trend and focus on this second term. Accordingly, we define the *energy* to be the variance of the detrended time series, so that the energy equals  $\frac{1}{N} \sum_{j=1}^J \|\mathbf{W}_j\|^2$  and is thereby partitioned with respect to scale. Using the detrended time series here is consistent with other methods for oscillatory signals; for example, autocorrelation and DFT are usually applied to time series after removing the trend. The premise is that we are interested in the oscillatory portion of the signal, while the trend represents a different process. Figure S4 illustrates this method.

### S.3 Analytic wavelet transform

To further illustrate how to interpret the AWT, Figure S5 displays a 2-dimension heat map and a 3-dimensional surface representing the AWTs of a sinusoid with varying frequency and also a sinusoid of varying amplitude. While the 2-dimensional heat map is more convenient on the printed page, the 3-dimensional view emphasizes the definition of the ridge as the curve connecting the maximum values.

Unlike real-valued transforms, the complex-valued AWT yields estimates for both the amplitude and phase. The AWT of the wheel-running record in Case Study #2 is shown in Figure 6 of the main text, along with period and amplitude estimates over time. We can also extract the phase over time, which is shown in Figure S6. Graphs of the AWT applied to wheel-running records of other female mice are shown in Figure S7, demonstrating the generality of the 4-5 day pattern measured by the AWT.

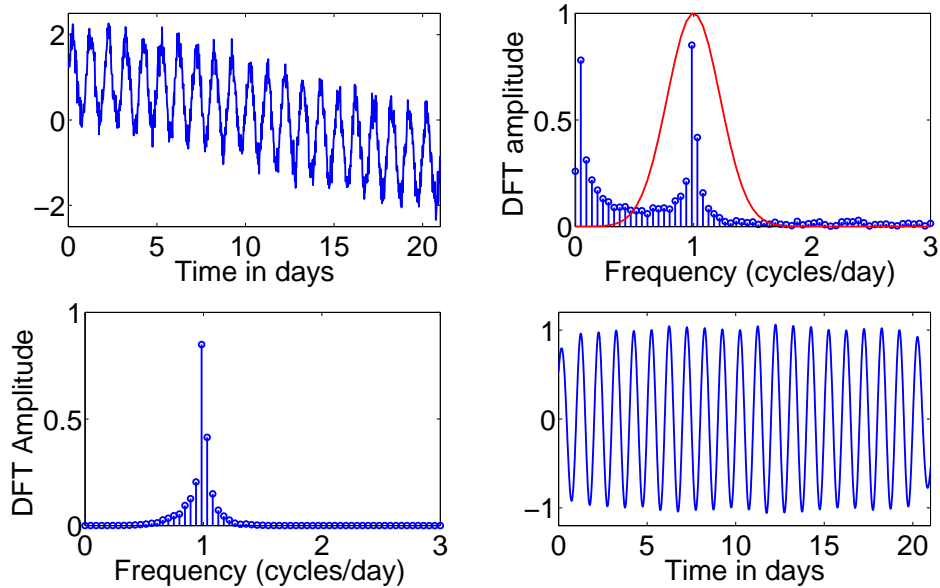


Figure S1: *Top left:* A sinusoid with 24h period and unit amplitude has white noise and trend added. *Top right:* The discrete Fourier transform (DFT) of the signal shows an amplitude of nearly 1 at the desired frequency of 1 cycle/day, but also has significant coefficients at low frequencies (from the added trend) and small jitter throughout the spectrum due to the added white noise. Also note the “leakage” around the peak circadian frequency. The resolution of the DFT depends on the number of cycles present in the signal; fewer cycles leads to more widely spread frequencies. If the signal’s peak frequency doesn’t exactly match one of the DFT’s frequencies, the DFT must use a combination of nearby frequencies to reconstruct the signal. By multiplying the DFT with the red curve, we retain the cluster of frequencies near the peak circadian frequency, but greatly reduce DFT coefficients corresponding to higher and lower frequencies. *Bottom left:* The result of multiplying the signal’s DFT coefficients by the red curve. Applying an inverse DFT to these new coefficients leads to a clean signal with diminished noise and trend. *Bottom right:* The filtered signal is very close to the original sinusoid before noise and trend were added. However, note the edge effects, including altered amplitude and frequency distortions, at the left and right ends. This is a general consequence of circular filters such as the DFT and the wavelet transforms if extra procedures to reduce edge effects are not taken. The problem is that circular filters wrap back around to the beginning of the signal when they reach the end of it, causing a discontinuity that distorts the transform coefficients.

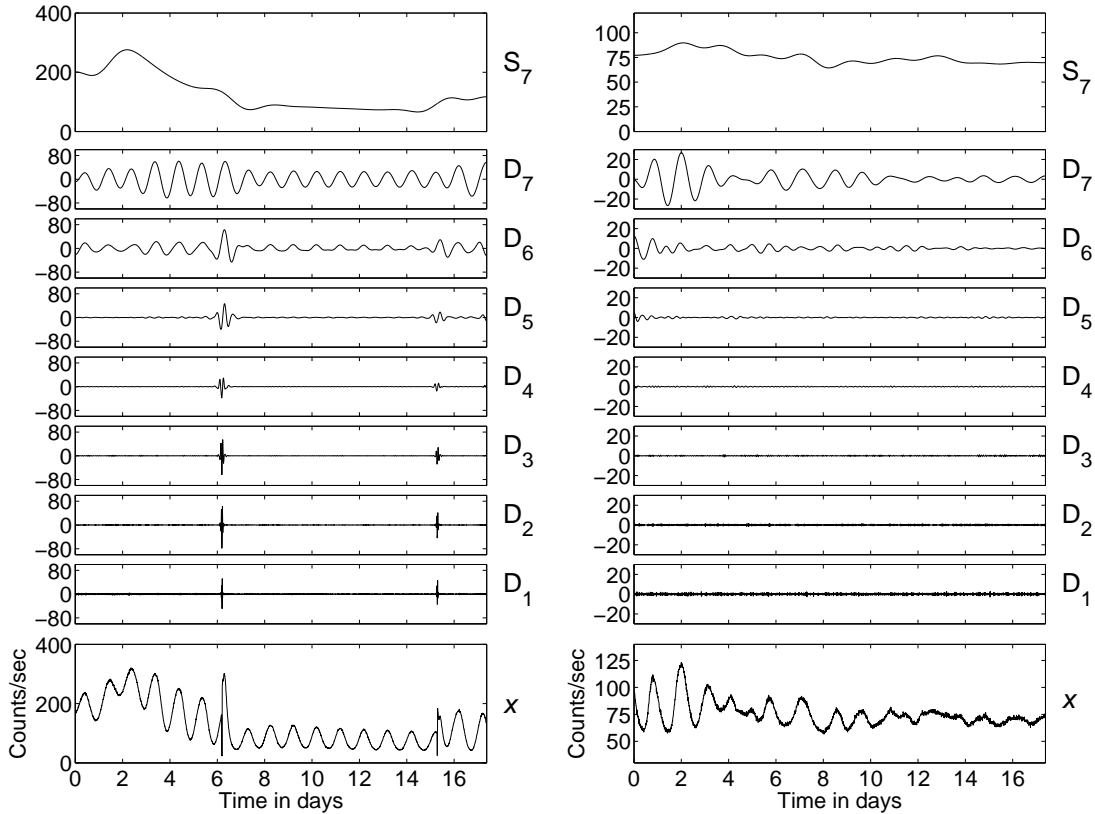


Figure S2: Multiresolution analysis of PER2::LUC bioluminescence rhythm from wild-type (left) and *Bmal1*<sup>-/-</sup> mutant (right) SCN explants (sampling interval  $\Delta t = 1/6$  h, units of photons/min), with data from Ko et al. (2010). The original signal  $x$ , shown at the bottom, is the sum of the wavelet details  $D_1 - D_7$  plus the wavelet smooth  $S_7$  that contains the trend. The detail  $D_k$  corresponds to a frequency band with period range  $2^k \Delta t$  to  $2^{k+1} \Delta t$  hours; in this example  $D_7$  corresponds to period range 21-42h. Rapid events like the media changes in the WT SCN time series on days 6 and 15 appear in details  $D_1 - D_3$  that correspond to very short scales. High frequency noise will be separated out into the small scale details,  $D_1 - D_3$  in this example.



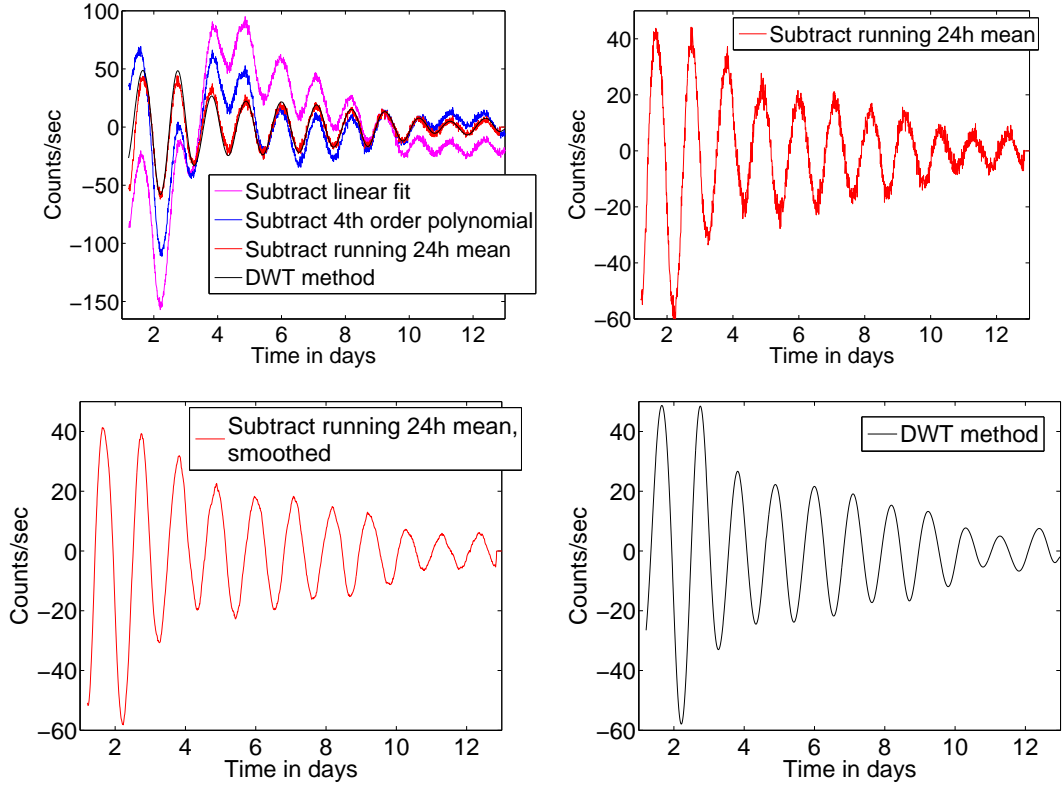


Figure S3: Comparison of methods to remove trend and noise, using the SCN explant PER2::LUC recording from an LD entrained female mouse shown in Figure 4C. The trend clearly does not follow an exponential or polynomial shape. Subtracting off a linear fit or 4th order polynomial fit make poor choices for detrending this time series, while subtracting a running 24h mean does as well as the DWT method of retaining the details corresponding to circadian periods. Notice that the DWT quite effectively removes noise as well as trend. Taking a running 2h mean to smooth after subtracting the running 24h mean does not remove the noise as well as the DWT method, particularly in the second half of the record. For purposes of, for example, peak-picking in order to compare cycle lengths, the DWT does an excellent job of preprocessing the data so that peak times can be easily determined.

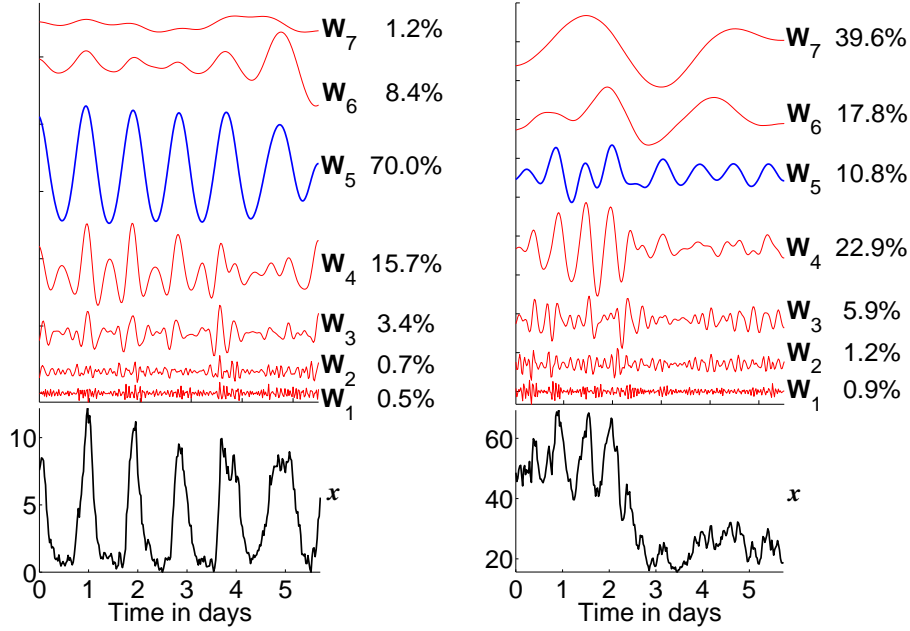


Figure S4: Wavelet coefficients from PER2::LUC bioluminescence rhythm from wild-type (left) and *Bmal1*<sup>-/-</sup> mutant (right) SCN cells (sampling interval  $\Delta t = 1/2$  h, units of photons/min), with data from Ko et al. (2010). All wavelet coefficient curves for a given cell have mean zero and are plotted with the same scale, so their magnitudes can be directly compared. Scaling coefficients are not shown. The level- $j$  wavelet coefficients  $\mathbf{W}_j$  corresponds to a frequency band with period range  $2^j \Delta t$  to  $2^{j+1} \Delta t$  hours; in this example  $\mathbf{W}_5$  corresponds to period range 16-32h. The partitioning of energy with respect to scale is one way to assess the strength of circadian rhythmicity in mutant cells. The percentage of energy contained in the level- $j$  wavelet coefficients is indicated along the right margin of each graph, and is defined by  $\|\mathbf{W}_j\|^2 / \sum_{i=1}^7 \|\mathbf{W}_i\|^2$ . For the wild-type SCN neuron shown on the left, 70% of the energy lies in the circadian component. For the *Bmal1*<sup>-/-</sup> SCN neuron shown on the right, only 11% of the energy lies in the circadian component, which strongly suggests that the cell is arrhythmic. Note that noise will typically have some energy throughout the spectrum and so will be present at all scales; a signal is rhythmic only if the energy in its circadian component is significantly above that of the other scales. In the case of this *Bmal1*<sup>-/-</sup> cell, the circadian component is almost surely due to noise, rather than any true circadian rhythm. Also observe the three large peaks occurring roughly 12h apart on the second day, which show up in  $\mathbf{W}_4$ , which corresponds to period range 8-16h.

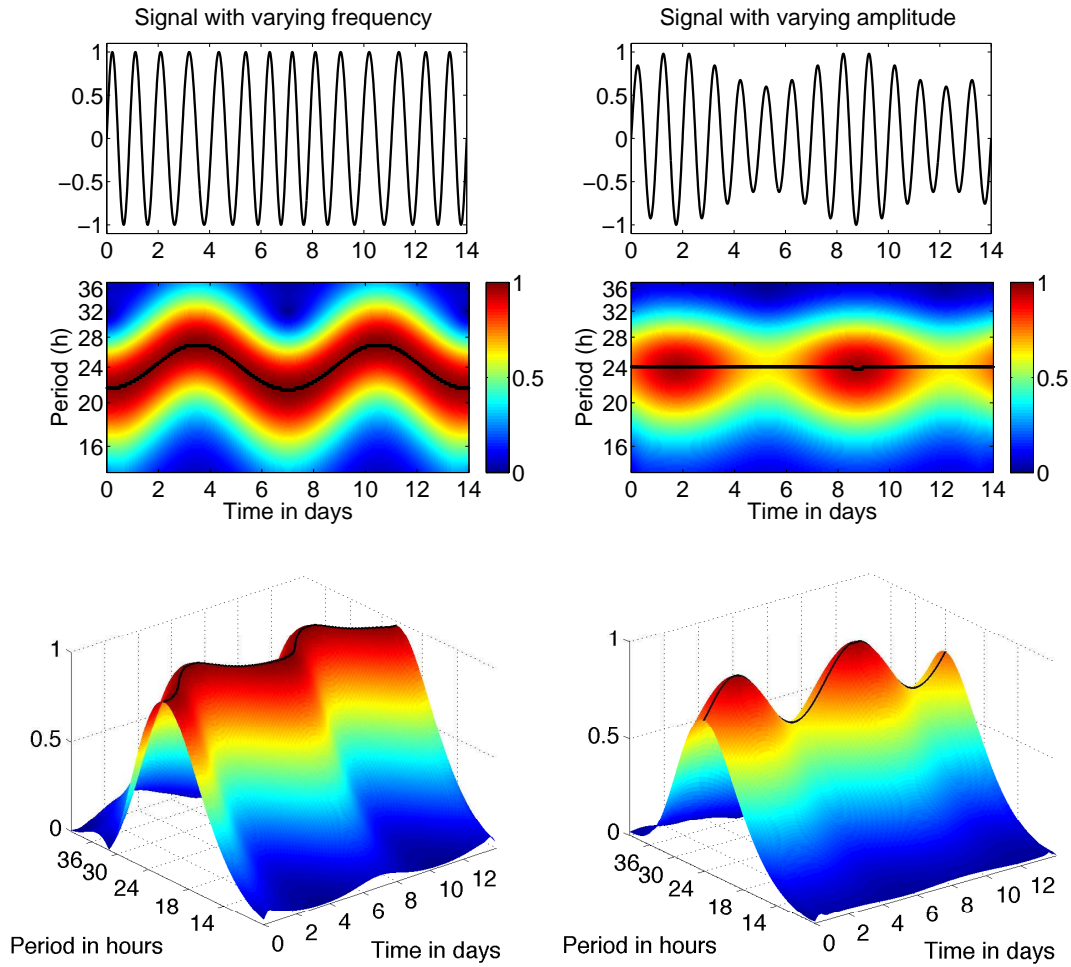


Figure S5: Two examples of signals (top) and their analytic wavelet transforms with ridges (middle and bottom). Left column involves a signal with frequency that varies over time, while the right column involves a signal with amplitude varying over time. Middle images show the absolute values of the AWT coefficients of the signals as a two-dimensional heat map, while the bottom images display the same values but as a 3-dimensional surface to emphasize the meaning of the wavelet ridge, which tracks the maximum coefficients over time. The color scale indicates the amplitude, while the wavelet ridge curves in black mark indicates the instantaneous frequency, written in terms of period= $2\pi$ /frequency for clarity. Periodic boundary conditions were used to eliminate edge effects.

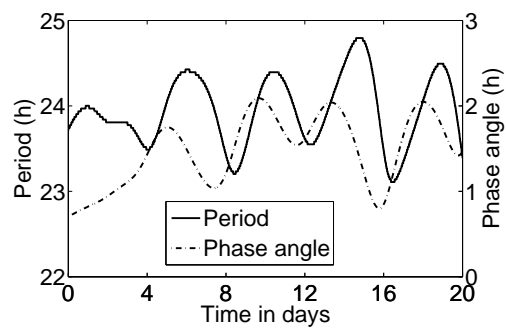


Figure S6: Wavelet ridge curve for period over time along with the corresponding phase angle of wheel-running activity with the LD cycle, showing the relationship between the 5-day variation in period and phase of wheel-running for the example shown in Figure 6 of the main text. A phase angle of 2h means that the mouse's internal clock is 2h ahead of ZT time, e.g., CT2 corresponds to ZT0. During this portion of the recording, the mouse is re-entraining to the LD cycle following an 8h advance, which may account for the first 4 days showing little of the 4-day pattern.

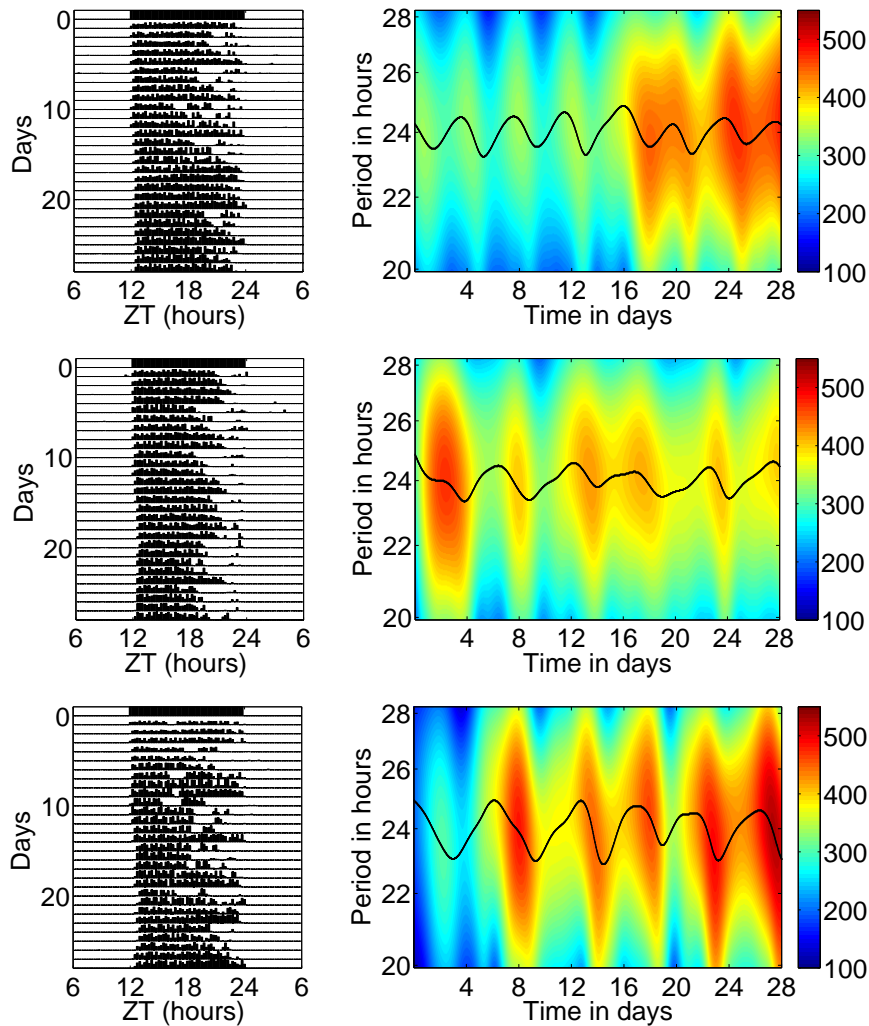


Figure S7: Three further examples of the AWT applied to wheel-running records of female mice. Actograms on the left show wheel-running (15 minute bins, ranging from 0 to 1200 revolutions per bin) under the LD cycle indicated by the white and black bars along the top. The AWT heat maps with ridges on the right quantify the 4-5 day variation in period and amplitude that is primarily due to changes in activity during the second half of the night. This analysis facilitates quantification of this pattern. For instance, activity amplitude is greatest (red color) when period is decreasing, as shown by the black ridge curve. (As in Figure S5, the color scale indicates the amplitude, while the wavelet ridge curves in black mark indicates the instantaneous frequency, written in terms of  $\text{period} = 2\pi / \text{frequency}$  for clarity. Two days were dropped on each side to eliminate edge effects.)